Electronic Journal of Structural Engineering

Original Article

Cite this: DOI:10.56748/ejse.25716

Received Date: 27 November 2024
Accepted Date: 22 February 2025

1443-9255
https://ejsei.com/ejse

The deformation and stress mechanism of water conveyance tunnel crossing strike-slip fault

Guangyue Ran[a*]
[a] China First Highway Xiamen Engineering Co., Ltd., Xiamen, 361021, China
*Corresponding author: 1091035861@qq.com

Abstract

Based on the Xianglushan water conveyance tunnel of the central Yunnan water diversion project, a large-scale finite element numerical model was established to study the lining deformation and failure mechanism of the Xianglushan water conveyance tunnel under the action of strike-slip faults. The lining damage law of the tunnel was revealed, and the corresponding fortification position was proposed, and the simulation result was validated experimentally. The results show that the displacement distribution of cross-fault tunnel under the action of strike-slip fault generally presents an elongated S-shaped distribution. In the fault fracture zone, the tensile failure is prevented at the arch waist convex from the fault dislocation surface, and the compressive failure is prevented at the concave. The range of compressive and tensile strains is mainly concentrated in the fault fracture zone ± 0.6 times the width of the fault zone. The shear damage of the top and bottom of the tunnel is relatively close. Therefore, combined with the strain distribution law of the left side and right-side walls of the tunnel and the maximum shear stress distribution law of the top and bottom of the tunnel, it is considered that the left and right-side walls located in the fault fracture zone should prevent tensile and compressive failure, and the top and bottom of the tunnel should prevent shear failure. The results of this study can provide a theoretical reference for the key vulnerable parts of the tunnel.

Keywords

Fault-crossing tunnel, Fault dislocation, Deformation profile, Mechanical mechanism, Fortification length

1. Introduction

With the arrangement of China's decision to build a strong transportation country, tunnel engineering has become one of the main ways to implement this major decision (Mei et al., 2021; Sun et al., 2020; Yang et al., 2021; Shen et al., 2020; Yang et al., 2020;). As a major promotion project of this huge system engineering, a line project in Southwest China will play an increasingly important role in the traffic networking plan. However, the geological conditions in Southwest China are relatively complex, and the terrain is undulating. Large number of faults, folds and other underground engineering poor quality occurrence environments are widely distributed (Zhu et al., 2021; Baziar et al., 2014; Bayati et al., 2017). The tunnel construction in Southwest China will face a very severe multiple damage test caused by earthquake, fault dislocation, high ground stress and large buried depth (Ryan et al., 2008; Durukal et al., 2002; Wang et al., 2001). The problem of the fault of the tunnel has also become a very important scientific research topic.

On January 8, 2022, an earthquake with a magnitude of Ms6.9 occurred in Menyuan County, Qinghai Province. The highest intensity reaches IX degrees (Chen et al., 2023). The earthquake caused serious damage to the surrounding bridge and tunnel projects, resulting in the interruption of high-speed rail operations from Lanzhou to Xinjiang. The epicenter of the earthquake is located on the south side of the fault of the Lenglongling fault on the Qinghai-Tibet Plateau, with a coordinate of 37.77° N, 101.26° E. The fault is a left-lateral strike-slip type with a focal depth of about 10 km. More than 20 earthquake events (including mainshocks and aftershocks) with M≥3 were recorded before and after the earthquake, and the distribution range was mainly concentrated along the Lenglongling fault (LLLF) and the Tuolaishan fault (TLSF).

During the Menyuan earthquake, two rupture zones were formed on the surface, with azimuth coordinates of 113 ° and 87 °, respectively, located in the western section of LLLF and the eastern section of TLSF. According to the post-earthquake survey, the fault structure is almost erect, resulting in a maximum surface horizontal displacement of about 2.8 m, mainly extending along the fault. At the same time, the surface rupture extends downward and crosses the beam tunnel, resulting in the destruction of the tunnel structure, especially at about 700 m from the tunnel entrance. According to the post-earthquake survey, the fault structure is almost erect, resulting in a maximum surface horizontal displacement of about 2.8 m, mainly extending along the fault. At the same time, the surface rupture extends downward and crosses the beam tunnel, resulting in the destruction of the tunnel structure, especially at about 700 m from the tunnel entrance. Influenced by the strong movement of the fault, there are different degrees of cracking, local falling block and overall dislocation failure in the tunnel. Influenced by the strong dislocation of the fault, there are different degrees of cracking, local falling block and overall dislocation failure in the tunnel, as shown in Fig. 1.

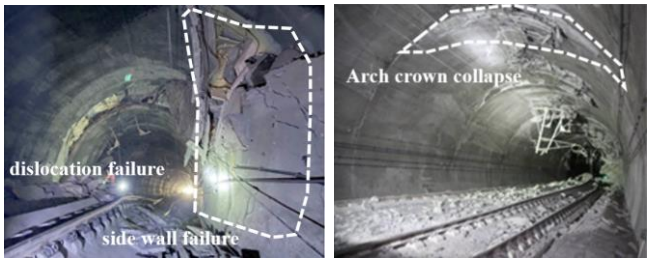

Fig. 1 Daliang tunnel disaster situation subjected to Menyuan earthquake

The relative motion of faults between crustal plates induces the occurrence of earthquakes. According to the dislocation mode of relative motion of faults, faults can be divided into normal faults, reverse faults and strike-slip faults, and can also be divided into stick-slip and creep-slip (Uckan et al., 2015; An et al. 2021; Zhong et al., 2020). For many years, the movement of faults has caused many underground projects such as tunnels to suffer serious dislocation disasters and threats (Kun et al., 2013), such as lining cracking, dislocation, hole collapse, etc. In the process of stick-slipping, faults promote intermittent rapid sliding between plates, which in turn leads to earthquakes. The 1971 San Fernando earthquake in the United States (Trifunac et al., 2004), the 1976 Tangshan earthquake in China (Roy et al., 2016), the 1995 Hanshin earthquake in Japan (Fukuyama et al., 2000), the 1999 Chi-Chi earthquake and the 2008 Wenchuan earthquake in China (Shen et al., 2014) all showed strong damage to the tunnel.

In view of this, scholars have carried out relevant research on fault dislocation and ground motion. According to the active direction of the fault, the fault is divided into normal fault, reverse fault and strike slip fault. According to the fault dislocation mode, it can be divided into stick slip and creep slip (Kiani et al, 2016). The research on the fault mechanism of the fault tunnel is mainly carried out through model test and numerical simulation. Majid K.et al. explored the influence of tunnel buried depth and fault dip angle on the structure of segmental tunnel under the action of normal fault through model test (Kiani et al, 2016). Lin et al. (2007) studied the deformation and failure characteristics of shield tunnel under the action of reverse fault by simulating the scale model test of shield tunnel crossing active fault under the action of reverse fault. Liu et al. (2015) obtained the response law and influence range of highway tunnels with different dip angles under normal/reverse fault stick-slip dislocation.

Based on centrifuge test and numerical simulation, Yao et al (2021) and Zeng et al. (2021) obtained the analysis results of the influence range of cross-fault tunnels under the action of reverse faults and strike-slip faults and believed that the influence range of tunnels is about 1.4-4.7 times the diameter of tunnels. Wang et al (2023) explored the progressive failure of tunnel crossing normal faulting and the anti-dislocation measurement of tunnel. Numerical simulation has the advantages of low cost, high flexibility, visualization and repeatability. Compared with the numerical simulation method, the model test method has higher cost, larger time consumption and larger scale limitation. Therefore, two methods are usually used in the study to verify the reliability of the results.

In summary, at present, there are few studies on the influence of tunnel under the action of strike-slip fault dislocation. It is necessary to carry out research on the forced influence of cross-fault tunnel structure under the action of strong earthquake-stick-slip dislocation, and more importantly the fortification length was concluded. Based on this, this paper establishes a three-dimensional numerical model of the corresponding cross-active fault and compares and analyzes the response law of the near-fault pulse-type ground motion to the tunnel structure under the premise of different dislocations. The simulation corrections have been verified based on the reported experimental test results. The research results of this paper can provide a research basis for exploring the deformation mechanism and failure mechanism of tunnels across active faults in the earthquake area and provide a research reference for the design of tunnels across faults in southwest China.

2. Background

2.1 Engineering introduction

The total length of the Xianglushan tunnel is 62.5 km. Affected by the surrounding topography and geological conditions; the tunnel crosses multiple fault zones. The Longpan-Qiaohou, Lijiang-Jianchuan and Heqing-Eryuan faults are Holocene regional active faults. Xianglushan tunnel is a typical tunnel crossing active fault, which is characterized by many active faults, frequent earthquakes and high intensity. The tunnel section of Xianglu Mountain crosses the watershed between Jinsha River and Lancang River. After investigation, the Longpan-Qiaohou fault zone is divided into three nearly parallel faults in the study area of Xianglushan tunnel. The main fault fracture zone and its influence bandwidth are more than 2 km. The Lijiang-Jianchuan tunnel passes through the part along the fault to form a trough with a width of 1 ~ 2 km, and the fracture breaking bandwidth is large.

2.2 Site characteristics

The Xianglushan tunnel of the central Yunnan water diversion project passes through the Lijiang-Jianchuan fault. After investigation, the fault zone is divided into several faults in the study area of Xianglushan tunnel. The tunnel passes through the part along the fault to form a trough with a width of 1 ~ 2 km, and the fracture breaking the bandwidth is large. The stratigraphic information of Lijiang-Jianchuan fault is complex and diverse, involving multiple geological ages and lithological characteristics (Fig. 2). Fault breccia is the main fault breccia in the fault area, covering the second member of the Triassic Beiya Formation and the Quaternary alluvium.

3. Simulation analysis model

3.1 Model establishment

In this study, the finite difference software FLAC3D was used to establish a three-dimensional cross-fault tunnel model. In order to avoid the error caused by the size effect, the model size is length × width × height: 300m×100m×100mm, and the width of the fault zone is set to 50m. The diameter of the tunnel is 11.20 m, and the lining thickness is 1.02 m. The model used in the calculation is shown in Fig. 3.

Based on the pseudo-static analysis method, the ground constraints on both sides of the active fault zone are as follows: One side of the ground is regarded as fixed. The other side simulates the dislocation of active faults by applying forced displacement. In order to simulate the contact between the fault surface and the surrounding rock and the lining in the rock mass medium, two kinds of rock mass interfaces are set in the model. Each interface is composed of a component interface unit, and an interface unit is composed of three nodes. Each interface unit allocates the area to its three nodes, and each interface has a corresponding representative area. The built-in constitutive model in FLAC3D software obeys the Coulomb shear strength criterion. The basic principle of the calculation is to obtain the normal absolute displacement and tangential relative velocity of each node in each time step and calculate the normal force and tangential force according to the constitutive model. When the maximum tensile stress of the normal spring between contacts exceeds the normal tensile strength, the connection between the surrounding rock and the lining will be disconnected. Different from normal mechanical behavior, tangential mechanical behavior is mainly characterized by that when the shear stress is greater than the shear strength, the shear stress remains unchanged, and the spring displacement will gradually increase. The mechanical parameters of the contact surface in the model are shown in Table 1, where the first surface presents the contact face between rock mass and tunnel, and the second surface presents the contact faces in the fault plane.

The constitutive model of lining selects the plastic model to represent the nonlinear characteristics subjected to strike-slip fault, and the strain-stress tension and compression relationship of the tunnel follows the curves as shown in Fig. 4.

The mechanism parameters of the simulation model are listed in Table 2, where the parameters include rock mass, fault and tunnel lining.

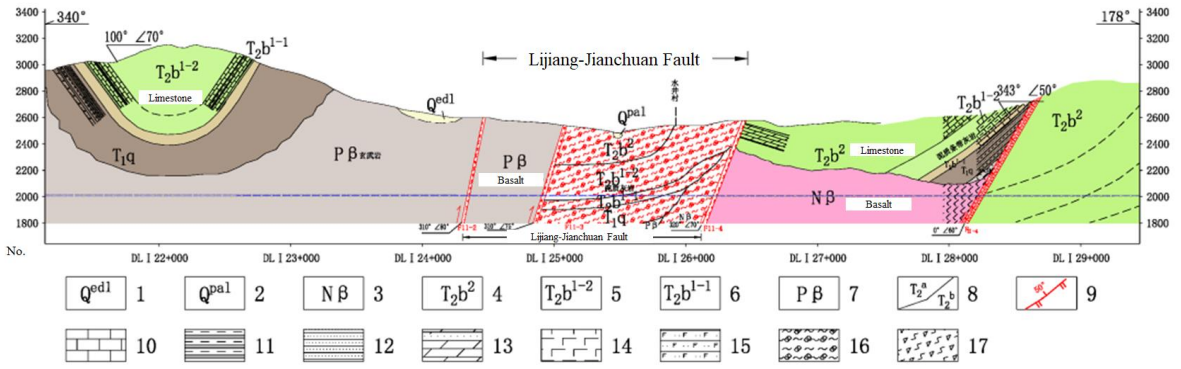

Fig. 2 Lijiang-Jianchuan fault around Xianglu Mountain tunnel site

(1. Quaternary residual slope layer; 2. Quaternary alluvial-proluvial layer; 3. Neogene basalts; 4. Triassic Beiya Formation second member; 5. Upper part of the first member of the Triassic Beiya Formation; 6. The lower part of the first member of the Triassic Beiya Formation; 7. Permian basalt; 8. Stratigraphic boundary; 9. thrust fault; 10. limestone; 11. Shale ; 12. Sandstone; 13. Argillaceous limestone; 14. Basalt; 15. Siltstone; 16. Fault breccia; 17. Fragmented rock)

Table 1. The strain-stress relationship of the contact faces

Number	k_n (MPa/m)	k_s (MPa/m)	f_t (MPa)	c (MPa)	φ (°)	Bonded slip on/off
1	2500	2500	0.5	1.8	59.6	on
2	3000	3000	1.3	1.6	50	off

Table 2. The strain-stress relationship of the concrete

Type	γ (kN m^{-3})	E (GPa)	ν	c (MPa)	φ (°)
Rock mass	20	10	0.3	0.85	30
Fault	19	8	0.35	0.10	20
lining	25	28.0	0.2	-	-

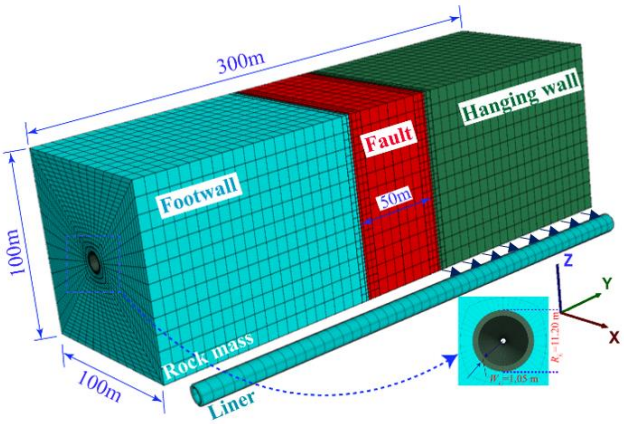

Fig. 3 Modelling establishment for fault dislocation analysis

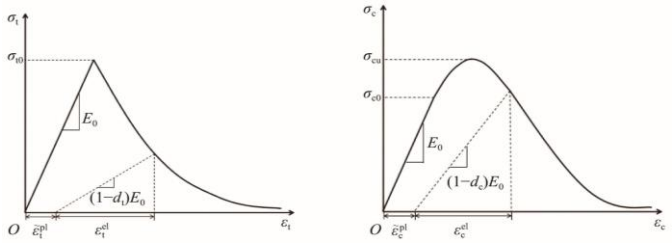

(a) Tension (b) Compression

Fig. 4 The strain-stress relationship of the concrete

3.2 Loading process

The tunnel is located in two walls and a fault fracture zone, forming a three-dimensional analysis model of surrounding rock-fault-tunnel. The ground motion and inertial force effect generated during the fault movement are ignored in the model. In the generalized model, the fault slip surface is in the middle of the fault fracture zone, and its contact property obeys the Mohr-Coulomb friction contact constitutive relationship. The quasi-static loading method is used to apply the forced displacement outside the boundary of the active plate to realize the fault dislocation loading. The boundaries in the foot wall of the model wad fixed, while the horizontal displacement boundaries were applied on the hanging wall. The bottom of the model keeps stability on the vertical direction.

The dislocation momentum input mechanism is based on the displacement of the project for one hundred years. The horizontal dislocation rate is applied to the node on the side of the tunnel moving plate. After completing a certain time step calculation, the dislocation results with dislocation momentum of 10 cm, 20 cm, 30 cm, 40 cm and 50 cm are obtained. As a preset model for ground motion analysis, seismic waves are input to the bottom of the model under the premise of 5-level dislocation, and the mechanism of tunnel dislocation response under the action of cross-active fault dislocation is studied.

4. Results

4.1 Tunnel deformation analysis

In the calculation, the dynamic response characteristics of the near-fault measured ground motion tunnel are studied under the condition of 10 cm, 20 cm, 30 cm, 40 cm and 50 cm five-order staggered momentum. Vazouras et al. (2010) considered that the axial displacement curve of tunnel lining under the action of strike-slip fault should satisfy the simple harmonic function relationship related to the two key parameters of fault displacement and fault zone width. The specific function relationship was listed as Equation 1:

$$u(x)=\frac{d}{2}\cos\beta(1-\cos\frac{\pi}{L}x) \quad (1)$$

where, d is the fault dislocation momentum, L is the width of the fault zone, and β is the angle between the fault plane and the vertical direction of the tunnel axis, in which β equals to 0 meaning the tunnel across the strike-slip fault, as shown in Fig. 5.

Fig. 6 shows the distribution nephogram of lining displacement is given when the fault displacement is 10 cm, 20 cm, 30 cm, 40 cm and 50 cm respectively.

From the distribution cloud diagram of lining displacement with fault dislocation momentum, under a certain dislocation momentum, the displacement of lining located in the movable plate and the fixed plate changes little along the longitudinal direction of the tunnel. The displacement increment of the two linings along the longitudinal direction of the tunnel is close to 0. The displacement of the lining in the fixed plate is small, and it can be considered that no displacement occurs. The lining displacement in the active plate changes obviously with the increase of fault dislocation momentum. The displacement value of the lining is equal to the displacement value of the same instantaneous fault displacement. The area where the displacement increment has a large value appears in the fault fracture zone, where the lining displacement changes greatly, and the overall distribution is 'S' type. Along the longitudinal direction of the tunnel, there are two inflection points at the left and right sides of the arch waist.

Fig. 7 shows the comparison of displacement distribution curves under different dislocations at the tunnel axis by numerical calculation and analytical expression.

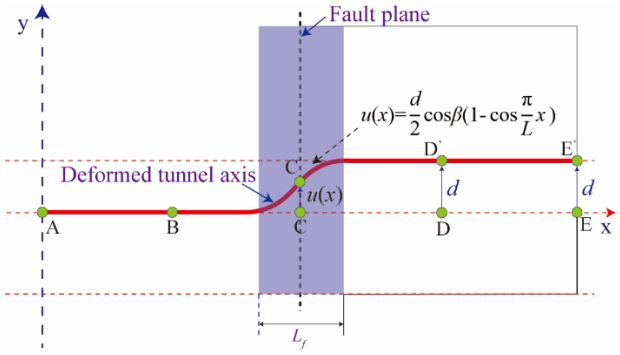

Fig. 5 Analytical solution of deformation mode of lining

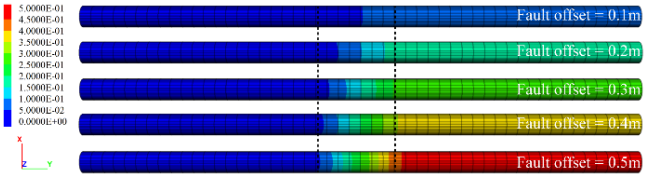

Fig. 6 The lining displacement contours under different fault offsets

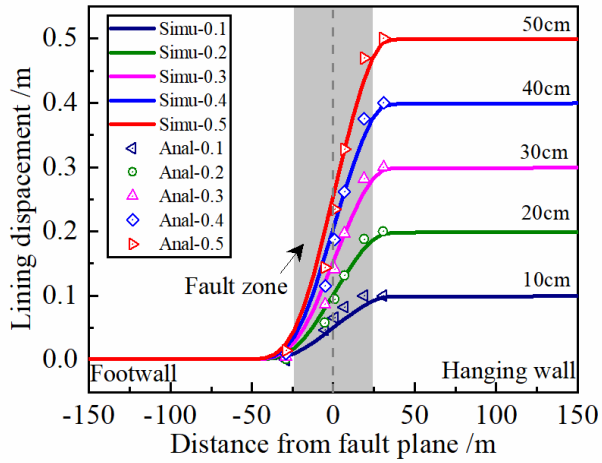

Fig. 7 Comparison of simulation result and analytical solution

From the simulation results of lining displacement, the lining presents an S-typed distribution. The displacement value of the lining located at the movable plate is equal to the input dislocation value, and the lining position in the fixed plate is relatively fixed. The lining displacement in the fault fracture zone transits longitudinally along the tunnel and to the active plate. The results are in good agreement with the analytical expression results of the existing literature.

4.2 Longitudinal stress analysis

Fig. 8 shows the longitudinal stress distribution curves of the side walls on the east and west sides of the lining with the amplification deformation coefficient of 50 under the dislocation of 10 cm, 20 cm, 30 cm, 40 cm, and 50 cm. The longitudinal stress distribution of the eastern wall of the tunnel is shown in Fig. 8a, and the longitudinal stress distribution of the right wall is shown in Fig. 8b.

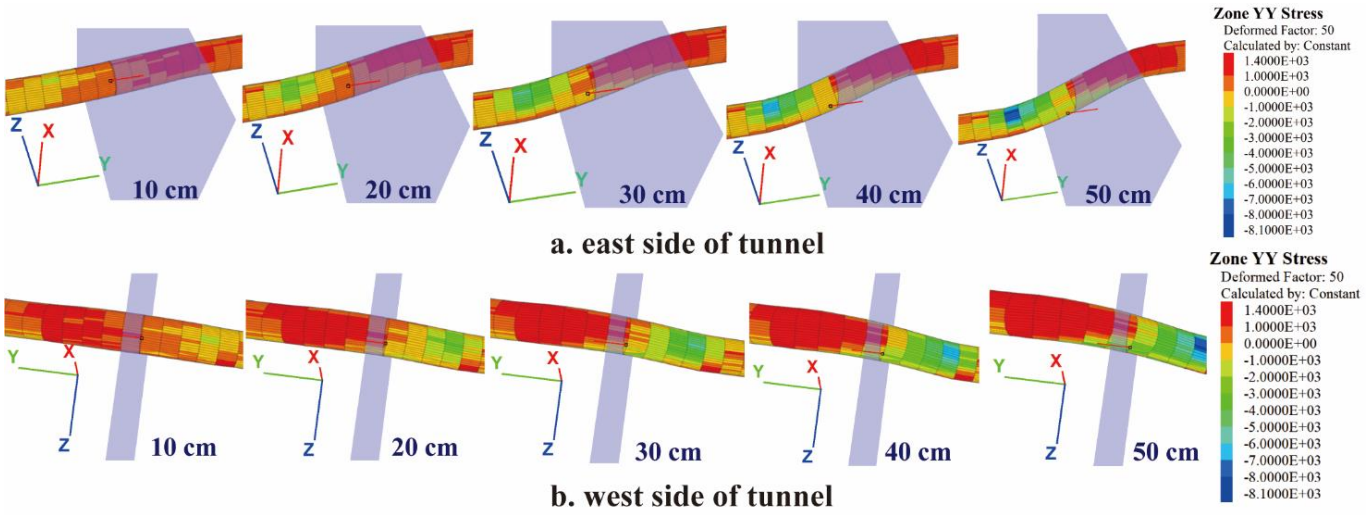

Fig. 8 The longitudinal stress of lining east and west sides under fault offset from 10cm to 50cm (KPa)

According to the longitudinal stress contours of lining east and west sides under fault offset from 10cm to 50cm, local longitudinal stress distribution curves at the left and right-side walls of the tunnel under different dislocations were presented in Fig. 9.

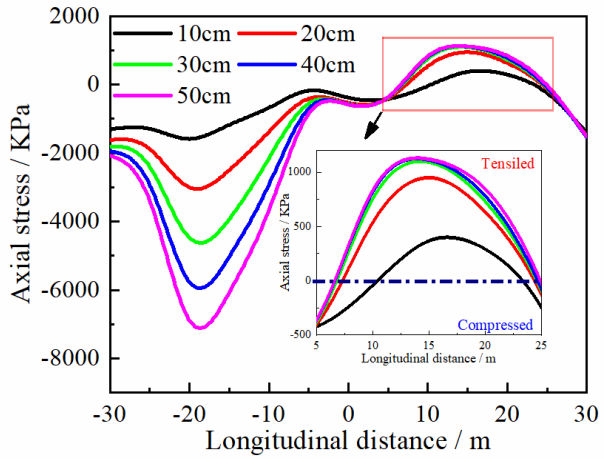

(a) east side of tunnel

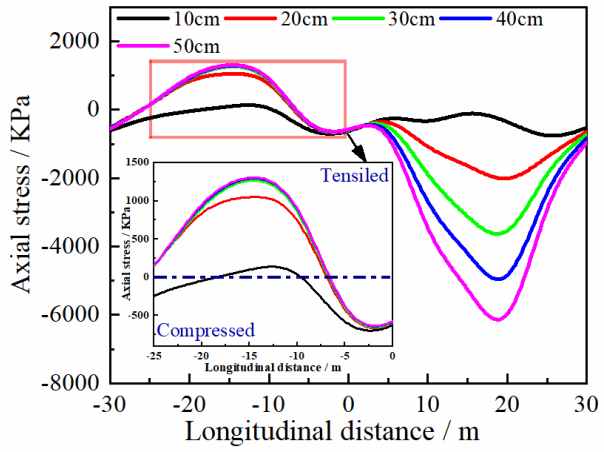

(b) west side of tunnel

Fig. 9 The local longitudinal stress distribution curves

From the longitudinal stress distribution given in Fig. 8 and Fig. 9, the longitudinal stress of the lining structure of the east and west side walls has the property of anti-symmetry. The compression on the west side of the lining on the side of the movable plate is more obvious, while the arch waist on the west side of the lining on the side of the fixed plate shows more serious tensile failure. On the contrary, the tension of the arch waist on the east side of the lining on the side of the movable plate is more obvious, while the arch waist on the east side of the lining on the side of the fixed plate is compressed. The results verify the conclusions of the literature.

With the increase of fault dislocation, the lining structure near the fault fracture zone bears compressive stress, and gradually increases with the increase of dislocation, but the increase is gradually decreasing. Before reaching the ultimate dislocation, the maximum compressive strains of the east and west side walls are 7.37 MPa and 6.07 MPa, respectively. The extreme point of compression appears at about 2.0D from the fault plane. Both are less than the ultimate compressive strength of C35 grade concrete. It shows that there is no serious compression damage during the fracture.

On the contrary, the tensile strain distribution of lining shows a certain distribution law. From the longitudinal strain distribution law of the eastern side wall, the lining structure on the side of the active plate is significantly damaged by tension and is greatly affected by fault dislocation. When the dislocation is 10 cm, the tensile stress on both sides is small, which does not reach the ultimate tensile strength design value of the established concrete grade. However, with the further application of fault dislocation, the tensile strain on both sides of the tensile area began to increase, especially on the tensile side of the western wall. The main reason for this phenomenon is that with the increase of the dislocation momentum, the surrounding rock void occurs near the tensile side of the west side wall. This phenomenon will be more conducive to the continued deformation of the lining structure on the tension side, resulting in a greater increase in the stress value when the dislocation momentum reaches 20 cm. Compared with the large stress increase on the tensile side of the west wall, the tensile stress area on the east wall is constrained by the surrounding rock pressure on the passive side, resulting in a relatively small increase in tensile stress in this area. It is worth noting that the distance between the extreme points of compression on both sides of the tunnel and the faulty plane is relatively consistent, which is about 1.5 times the diameter of the tunnel.

With the further increase of dislocation, compressive stress gradually increases, and the compressive stress gradually increases to the ultimate tensile stress value of the established concrete grade of 1.4 MPa. When the dislocation reaches 30 cm, tensile cracks caused by tensile deformation begin to appear on both sides of the lining structure. After that, the tensile stress will not continue to increase when the value of the mis-momentum is applied.

4.3 Shear stress analysis

The ratio of shear strength to compressive strength of concrete ranges from 0.095 to 0.121, and the shear modules are about 40 % of the elastic modules of concrete. Therefore, the shear strain value should meet the relationship as shown in Equation 2.

$$\varepsilon_s = \frac{\tau}{G} = \frac{0.121\sigma_u}{0.4E_c} \quad (2)$$

where "τ" is the shear force and G is shearing modulus. "σ" _"u" and "E" _"c" represents the compressive strength and elastic modulus of concrete. According to the parameters of the selected concrete strength of the tunnel engineering, the maximum shear strains are 0.18‰. The cloud diagram and curve of shear strain distribution at the crown and invert of the lining under different dislocations are shown in Fig.10.

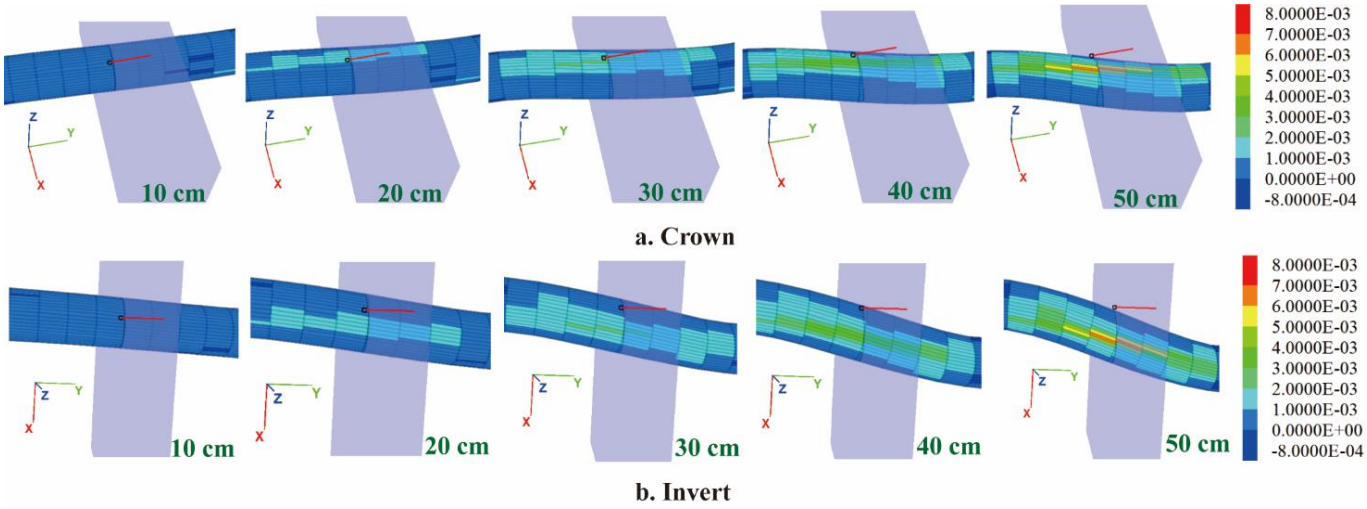

Fig. 10 The shear strains contours of tunnel crown and invert

According to the shear strains contours of tunnel crown and invert, local shear strains curves of tunnel crown and invert under different dislocations were presented in Fig. 11.

From Fig.10 and Fig.11, it can be seen that the shear strain distribution at the top and bottom of the tunnel is antisymmetric. The maximum shear strain peak is mainly concentrated near the fault plane, and the maximum shear strain gradually increases with the increase of fault dislocation. According to the shear strain calculation equation, the shear strain value is 1.6×10-4, which is obviously smaller than the peak shear strain at the top and bottom of the cave. Therefore, the roof and bottom of the lining structure at the fault fracture zone are subjected to more serious shear failure under the action of strike-slip fault dislocation.

4.4 Validation with experimental test

Under the same analysis conditions, Zhou et al. (2021) discussed the progressive failure mode of tunnels under the action of strike-slip faults. The device used in the study is a self-designed test model box that can simulate strike-slip faults by adjusting the dislocation speed of the model box. The design size of the box is 72 cm × 50 cm × 40 cm, and the loading system of the test device is realized by the jack acting on the outside of the movable plate box. By comparing the numerical simulation results with the model test results, it is found that the deformation modes of the tunnel under the two methods are in good agreement, as shown in Fig. 12. Furthermore, it can be found that the stress concentration area in the numerical simulation is in good agreement with the failure part of the model test tunnel.

The tunnel structure is seriously damaged when it is subjected to strike-slip fault dislocation. The deformation of the lining is mainly concentrated on the fault zone. Due to the extrusion of the rock mass, the circular section of the tunnel becomes elliptical. The failure mode of the lining is the combined action of shear failure and bending failure.

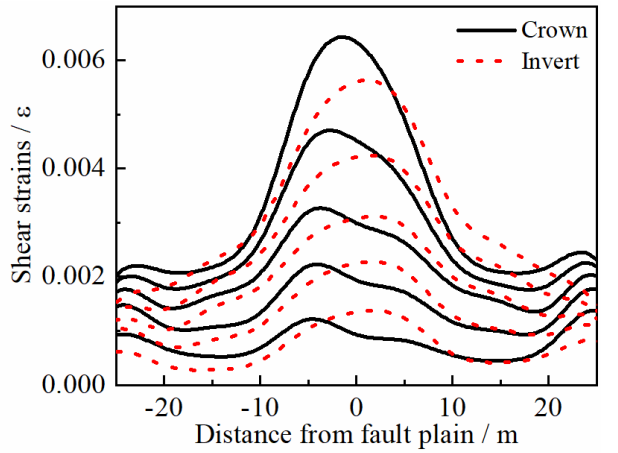

Fig. 11 The local shear strains curves of tunnel crown and invert

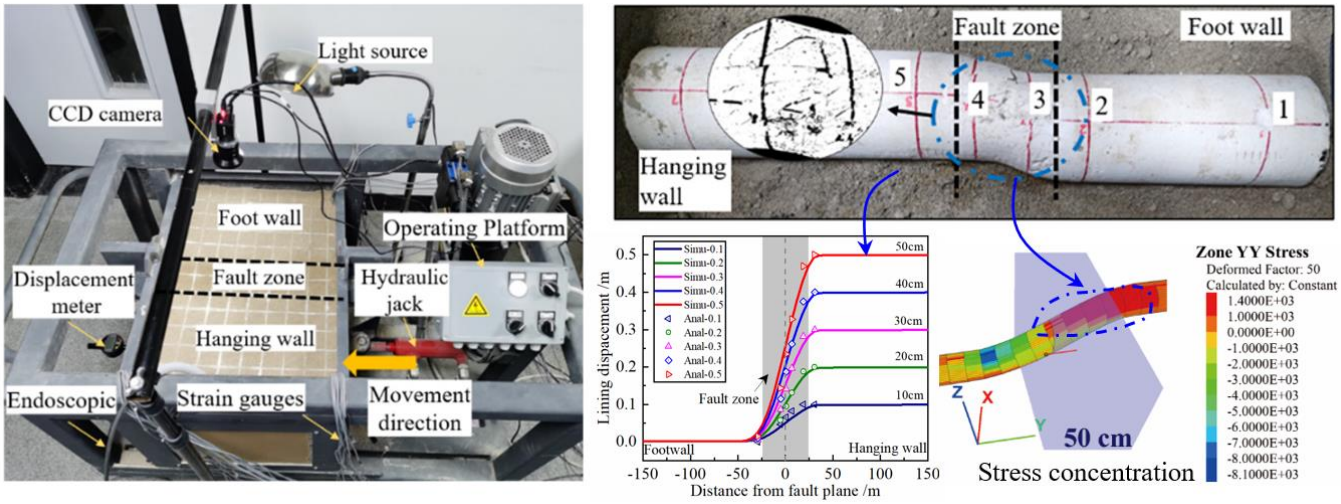

Fig. 12 The validated results and the numerical results

5. Conclusions

In this paper, the dislocation response of a real water conveyance tunnel crossing strike-slip fault was investigated. A three-dimensional numerical model considering the nonlinear feather of tunnel subjected to the fault dislocation was built, where the contact relationship of tunnel-rock mass and fault-rock mass were considered. And the simulation model was loaded with a quasi-static loading mode. Based on the simulation model, the displacement and shear mechanism of tunnel were deeply revealed. The conclusions are as follows:

[1] Based on the verified results, the displacement distribution of cross-fault tunnel under the action of strike-slip fault generally presents an elongated S-shape distribution, which can be fitted well with harmonic function relationship. The lining displacement value located on the fixed plate is about the real-time fault dislocation displacement input value. The lining displacement in the fixed plate is relatively fixed, while the lining displacement in the fault fracture zone is distributed along the longitudinal distance of the tunnel.

[2] The longitudinal strain of the left and right-side walls: the fragmentation is obvious, and the displacement distribution of the two plates is uniform. In the fault fracture zone, the tensile failure is prevented at the arch waist convex from the fault dislocation surface, and the compressive failure is prevented at the concave. The range of compressive and tensile strains is mainly concentrated in the fault fracture zone ± 0.6Wf (Wf is the width of the fault zone).

[3] The lining roof and bottom of Xianglushan water conveyance tunnel located in the fault fracture zone bear large shear stress, and the maximum shear stress appears near the fault dislocation surface. The maximum yield stress involves the range of-0.5Wf ~ 0.5Wf, and the shear damage of the top and bottom of the tunnel is relatively close. Therefore, combined with the strain distribution law of the left and right-side walls of the tunnel and the maximum shear distribution law of the top and bottom of the tunnel, it is considered that the left and right-side walls located in the fault fracture zone should prevent tensile and compressive failure, and the top and bottom of the tunnel should prevent shear failure. The research results are concluded based on the numerical simulation and experimental test, and the further verification and anti-dislocation application in the real-world tunnel engineering should be the further research target.

Acknowledgement and Supplementary data

This research did not receive any specific grant from funding agencies in the public, commercial, or not-for-profit sectors. The authors are grateful to anonymous reviewers for their valuable and most helpful comments.

Reference

MEI X, SHENG Q, CUI Z, et al. Effect of Near-Fault Pulsed Ground Motions on Seismic Response and Seismic Performance to Tunnel Structures [J]. Shock and Vibration, 2021, 2021: 1-18. https://doi.org/10.1155/2021/9999007

SUN B, ZHANG S, DENG M, et al. Inelastic dynamic response and fragility analysis of arched hydraulic tunnels under as-recorded far-fault and near-fault ground motions [J]. Soil Dynamics and Earthquake Engineering, 2020, 132. https://doi.org/10.1016/j.soildyn.2020.106070

YANG Y, YU H, YUAN Y, et al. 1 g Shaking table test of segmental tunnel in sand under near-fault motions [J]. Tunnelling and Underground Space Technology, 2021, 115. https://doi.org/10.1016/j.tust.2021.104080

SHEN Y S, WANG Z Z, YU J, et al. Shaking table test on flexible joints of mountain tunnels passing through normal fault [J]. Tunnelling and Underground Space Technology, 2020, 98. https://doi.org/10.1016/j.tust.2020.103299

YANG H, LIU C, JIANG X, et al. Shaking Table Test and Numerical Simulation for Dynamic Response of Shallow-Buried Bias Double-Arch tunnel [J]. Geotechnical and Geological Engineering, 2020, 38(4): 3915-29. https://doi.org/10.1007/s10706-020-01267-9

ZHU D, ZHU Z, ZHANG C, et al. Shaking Table Test on the Tunnel Dynamic Response under Different Fault Dip Angles [J]. Symmetry, 2021, 13(8). https://doi.org/10.3390/sym13081375

BAZIAR M H, NABIZADEH A, JUNG LEE C, et al. Centrifuge modeling of interaction between reverse faulting and tunnel [J]. Soil Dynamics and Earthquake Engineering, 2014, 65: 151-164. https://doi.org/10.1016/j.soildyn.2014.04.008

BAYATI M, KHADEMI HAMIDI J. A case study on TBM tunnelling in fault zones and lessons learned from ground improvement [J]. Tunnelling and Underground Space Technology, 2017, 63: 162-70. https://doi.org/10.1016/j.tust.2016.12.006

Ryan H F, Parsons T, Sliter R W. Vertical tectonic deformation associated with the San Andreas fault zone offshore of San Francisco, California[J]. Tectonophysics, 2008, 457(3-4): 209-223. https://doi.org/10.1016/j.tecto.2008.06.011

Durukal E. Critical evaluation of strong motion in Kocaeli and Du¨zce (Turkey) earthquakes[J]. Soil Dynamics and Earthquake Engineering, 2002(22): 589–609. https://doi.org/10.1016/s0267-7261(02)00014-3

Wang W, Wang T, Su J, et al. Assessment of damage in mountain tunnels due to the Taiwan Chi-Chi Earthquake[J]. Tunnelling and Underground Space Technology, 2001, 16(3): 133-150. https://doi.org/10.1016/s0886-7798(01)00047-5

P. Chen, P. Geng, J. Chen, W. Gu, the seismic damage mechanism of Daliang tunnel by fault dislocation during the 2022 Menyuan Ms6.9 earthquake based on unidirectional velocity pulse input, Engineering Failure Analysis. 145(2023), 107047. https://doi.org/10.1016/j.engfailanal.2023.107047

UCKAN E, AKBAS B, SHEN J, et al. A simplified analysis model for determining the seismic response of buried steel pipes at strike-slip fault crossings [J]. Soil Dynamics and Earthquake Engineering, 2015, 75(55-65. https://doi.org/10.1016/j.soildyn.2015.03.001

AN S, TAO L J, HAN X C, et al. Application of two-level design method on subway tunnel crossing active fault: a case study on Urumqi subway tunnel intersected by reverse fault dislocation [J]. Bulletin of Engineering Geology and the Environment, 2021, 80(5): 3871-84. https://doi.org/10.1007/s10064-021-02164-y

ZHONG Z, WANG Z, ZHAO M, et al. Structural damage assessment of mountain tunnels in fault fracture zone subjected to multiple strike-slip fault movement [J]. Tunnelling and Underground Space Technology, 2020, 104 https://doi.org/10.1016/j.tust.2020.103527

KUN M, ONARGAN T. Influence of the fault zone in shallow tunneling: A case study of Izmir Metro Tunnel [J]. Tunnelling and Underground Space Technology, 2013, 33: 34-45. https://doi.org/10.1016/j.tust.2012.06.016

TRIFUNAC M D, TODOROVSKA M I. 1971 San Fernando and 1994 Northridge, California, earthquakes: did the zones with severely damaged buildings reoccur? [J]. Soil Dynamics and Earthquake Engineering, 2004, 24(3): 225-39. https://doi.org/10.1016/j.soildyn.2003.11.006

ROY N, SARKAR R. A Review of Seismic Damage of Mountain Tunnels and Probable Failure Mechanisms [J]. Geotechnical and Geological Engineering, 2016, 35(1): 1-28. https://doi.org/10.1007/s10706-016-0091-x

FUKUYAMA H, SUGANO S. Japanese seismic rehabilitation of concrete buildings after the Hyogoken-Nanbu Earthquake [J]. Cement & Concrete Composites, 2000, 22: 59-79. https://doi.org/10.1016/s0958-9465(99)00042-6

WANG W, WANG T, SU J, et al. Assessment of damage in mountain tunnels due to the Taiwan Chi-Chi Earthquake [J]. Tunnelling and Underground Space Technology, 2001, 16(3): 133-50. https://doi.org/10.1016/s0886-7798(01)00047-5

SHEN Y, GAO B, YANG X, et al. Seismic damage mechanism and dynamic deformation characteristic analysis of mountain tunnel after Wenchuan earthquake [J]. Engineering Geology, 2014, 180: 85-98. https://doi.org/10.1016/j.enggeo.2014.07.017

KIANI M, AKHLAGHI T, GHALANDARZADEH A. Experimental modeling of shallow segmental tunnels in alluvial affected by normal faults [J]. Tunnelling and Underground Space Technology, 2016, 51: 108-19. https://doi.org/10.1016/j.tust.2015.10.005

LIN M L, CHUNG C F, JENG F S, et al. The deformation of overburden soil induced by thrust faulting and its impact on underground tunnels [J]. Engineering Geology, 2007, 92(3-4): 110-132. https://doi.org/10.1016/j.enggeo.2007.03.008

LIU X Z, LI X F, SANG Y L, et al. Experimental study on normal fault rupture propagation in loose strata and its impact on mountain tunnels [J]. Tunnelling and Underground Space Technology, 2015, 49: 417-25. https://doi.org/10.1016/j.tust.2015.05.010

YAO C, HE C, TAKEMURA J, et al. Active length of a continuous pipe or tunnel subjected to reverse faulting [J]. Soil Dynamics and Earthquake Engineering, 2021, 148. https://doi.org/10.1016/j.soildyn.2021.106825

ZENG G, GENG P, GUO X, et al. An anti-fault study of basalt fiber reinforced concrete in tunnels crossing a stick-slip fault [J]. Soil Dynamics and Earthquake Engineering, 2021, 148. https://doi.org/10.1016/j.soildyn.2021.106687

Wang T, Geng P, Li P, et al. Deformation and failure of overburden soil subjected to normal fault dislocation and its impact on tunnel[J]. Engineering Failure Analysis, 2022, 142: 106747. https://doi.org/10.1016/j.engfailanal.2022.106747

VAZOURAS P, KARAMANOS S A, DAKOULAS P. Finite element analysis of buried steel pipelines under strike-slip fault displacements [J]. Soil Dynamics and Earthquake Engineering, 2010, 30(11): 1361-76. https://doi.org/10.1016/j.soildyn.2010.06.011

Zhou G, Sheng Q, Cui Z, et al. Investigating the deformation and failure mechanism of a submarine tunnel with flexible joints subjected to strike-slip faults[J]. Journal of Marine Science and Engineering, 2021, 9(12): 1412. https://doi.org/10.3390/jmse9121412

Disclaimer